University of Heidelberg
Department of Physics and Astronomy

Bachelor Thesis in Physics
submitted by

Thomas Gläßle

born
in Reutlingen (Germany)
on 22. March 1988

About

Spectrum guided integration for nonrelativistic quantum-mechanical problems

This Bachelor Thesis has been carried out by Thomas Gläßle

at the Max-Planck Institut für Kernphysik in Heidelberg
under the supervision of

Hon.-Prof. Dr. Keitel

Abstract
The numerical integration of the Schrödinger equation is an enduring challenge for modern computer algorithms. Today, many numerical schemes with different numerical properties are available for its solution. A complementary approach is to alter the physical description of the problem to improve the numeric performance of the used integration algorithm. The spectrum-guided-integration utilizes a gauge transformation to render the wave function easier to master for numerical algorithms. This method has proven to be of particular value if the quantum system behaves much like its classical analogon. In this thesis the technique is generalized for usage on systems that may feature strong quantum effects. An estimate of the error improvement is discussed. To illustrate and check the considerations, the methods are applied in three model systems. These are the harmonic oscillator, a laser interaction with a bound state in a softcore potential and a scattering event with a central softcore potential.

Zusammenfassung
Die numerische Integration der Schrödinger-Gleichung stellt eine fortwährende Herausforderung an moderne Computer-Algorithmen dar. Heute stehen viele numerische Schemen mit unterschiedlichen Prioritäten zu ihrer Lösung bereit. Ein komplementärer Ansatz besteht darin, die physikalische Beschreibung zu ändern, um die numerische Leistung des verwendeten Algorithmus zu verbessern. Die Spectrum-Guided-Integration passt die Wellenfunktion mithilfe einer Eichtransformation so an, dass sie von numerischen Algorithmen leichter zu verarbeiten ist. Diese Methode zeigt ihre Stärken vor allem in Systemen, welche sich ähnlich ihrem klassischen Analogon verhalten. In dieser Arbeit wird die Technik für Anwendung in Systemen erweitert, die auch starke Quanteneffekte aufweisen können. Die Verbesserung des Fehlers wird abgeschätzt. Eine Illustration und Prüfung der Erwägungen erfolgt an drei Modellsystemen: dem harmonischen Oscillator, einer Laser-Wechselwirkung mit einem gebundenen Zustand in einem Softcore-Potential, sowie einem Streuungsvorgang an einem Softcore-Potential.

Contents

1 Introduction

Quantum mechanics has contributed a lot to our understanding of nature. Unfortunately, there are only a few quantum mechanical problems of physical relevance which can be solved analytically. Therefore, numerical methods belong to the theory since its beginnings [1]. The development of modern computer technology made it possible to calculate solutions for more complicated systems than anytime before.

Today, the numerical solution of the time-dependent Schrödinger equation is a common procedure. This method has the advantage, that it does not rely on approximations based on conjectures about the behaviour of the wave function. However, to model infinite systems on finite machines, a discretization of the wave function is required. Errors are therefore a natural part of any numerical solution. To some extent, this can be thought of as the result of the limitations imposed by the sampling theorem. In principle, the exact solution can be approximated to arbitrary precission by using a discretization of sufficiently high resolution. Of course, this requires a divergent computational effort.

Methods are desirable which yield accurate results while keeping the computational cost affordable. Many integration schemes with individual properties are available today. When chosing the appropriate algorithm for a particular task, apparent features to keep in mind include applicability, error scaling, performance as well as stability [2]. Another consideration sometimes receives less attention: The physical description of the wave function itself can have major influence on the outcome of the calculation. Canonical transformations provide means to alter the representation of the wave function and exploit system symmetries. In particular, the choice of an adjusted gauge is known to be of great importantance in this context [3].

This thesis focusses mainly on a technique called “spectrum-guided integration” and its application. The technique was developed by Bauke and Keitel [4]. The general idea of this method is to reduce the time-spatial oscillations of quantum mechanical wave functions by means of gauge transformations. The oscillations are reduced mainly in regions of high density of the wave functions. This yields good results for both stability and error reduction.

However, the method requires knowledge of the center-of-mass motion and the time evolution of the energy. For some systems these can be approximated by the classical solution. The Ehrenfest-theorem states that the center-of-mass motion of a narrow wave packet satisfy equations which are similar to Newton’s laws [5]. The classical analogon, however, is not always useful and sometimes not available at all. In this work a technique will be presented which is accessible even in those cases.

There are also systems for which the spectrum-guided-integration is unlikely to give major improvements in terms of accuracy. This is a consequence of its focus on the

center-of-mass motion. A generalization of the method is proposed which works in a similar way, but does not rely on physical observables.

This thesis is organized as follows: The purpose of Chapter 2 is to give a short review of quantum mechanics and explain the fundamental limits of numerical algorithms to solve the Schrödinger equation. In Chapter 3 the basics of the spectrum-guided-integration are explained, before two generalizations of the method are introduced. Numeric results for three examples are presented in Chapter 4 along with some benchmarks. Finally, Chapter 5 contains a resume and some final remarks.

2 Theoretical considerations

2.1 Nonrelativistic quantum mechanics

Quantum mechanics is a theory which explains many of the phenomena which are insufficiently described by classical physics. For example wave-like properties of particles and discrete values of observables are natural consequences of the theory.

In nonrelativistic quantum mechanics a state can be represented by a ray $|\Psi\rangle$ in a Hilbert-space $\mathcal{H}$. Observables O become hermitian operators $\hat{O}$. Time evolution is governed by the Schrödinger equation, which in its abstract form is given by

$$i\hbar\frac{\partial}{\partial t}\left|\Psi(t)\right\rangle = \hat{H}\left|\Psi(t)\right\rangle. \tag{2.1}$$

Here $\hat{H}$ is the Hamiltonian associated with the problem at hand and $\hat{E} = i\hbar\frac{\partial}{\partial t}$ is the energy operator. Equation (2.1) can be formally solved to give [6]

$$\left|\Psi(t)\right\rangle = \hat{T}\exp\left(-\frac{i}{\hbar}\int_0^t \hat{H}(\tau)\,d\tau\right)\left|\Psi(0)\right\rangle \tag{2.2}$$

where $\hat{T}$ denotes Dyson's time-ordering operator. It is possible to neglect the time-ordering for small time steps Δt:

$$\left|\Psi(t+\Delta t)\right\rangle = \exp\left(-\frac{i}{\hbar}\int_t^{t+\Delta t}\hat{H}(\tau)d\tau\right)\left|\Psi(t)\right\rangle + \mathcal{O}\left((\hat{H}\Delta t)^3\right). \tag{2.3}$$

The error is shown to be of third order by Pechukas and Light [7]. For time-independent Hamiltonians, obviously, the above formula is exact

$$\left|\Psi(t+\Delta t)\right\rangle = \exp\left(-\frac{i}{\hbar}\hat{H}\Delta t\right)\left|\Psi(t)\right\rangle. \tag{2.4}$$

Electromagnetism A particle in an electromagnetic field $(\boldsymbol{E}, \boldsymbol{B})$ is described by a Hamiltonian of the form

$$\hat{H} = \frac{1}{2m}\left(\hat{\boldsymbol{p}} - \frac{q}{c}\hat{\boldsymbol{A}}\right)^2 + q\hat{\phi}, \tag{2.5}$$

where the electromagnetic potentials $(\phi, \boldsymbol{A})$ determine the fields

$$\boldsymbol{E} = -\partial_{\boldsymbol{x}}\phi - \tfrac{1}{c}\partial_t\boldsymbol{A}, \tag{2.6a}$$
$$\boldsymbol{B} = \partial_{\boldsymbol{x}} \times \boldsymbol{A}. \tag{2.6b}$$

In spatial representation the Schrödinger equation Eq. (2.1) then becomes

$$i\hbar\frac{\partial}{\partial t}\Psi(\boldsymbol{x},t) = \frac{1}{2m}\left(-i\hbar\frac{\partial}{\partial \boldsymbol{x}} - \frac{q}{c}\boldsymbol{A}(\boldsymbol{x},t)\right)^2 \Psi(\boldsymbol{x},t) + q\phi(\boldsymbol{x},t)\,\Psi(\boldsymbol{x},t), \tag{2.7}$$

where $\Psi(\boldsymbol{x},t) = \langle \boldsymbol{x} \mid \Psi(t)\rangle$ is used as a shorthand for the projection onto configuration space.

2.2 The Sampling Theorem

The sampling theorem states that a function $f(t)$ can be reconstructed from a countable set of samples $f(t_i)$ if its integral transform $\mathcal{F}$ has compact support. There are many versions of the sampling theorem using various integral transforms. A good overview is given in an article of Abdul J. Jerri [8].

Shannon Sampling Theorem In Shannon's formulation [9] the *Fourier* transform $\mathcal{F}$ of the real function f is required to vanish outside an interval $[-W, W]$:

$$f(t) = f_W(t) \equiv \frac{1}{2\pi}\int_{-W}^{W} \mathcal{F}(\omega)\, e^{i\omega t} d\omega. \tag{2.8}$$

If this requisite is fulfilled f can be reconstructed based on an equidistributed series $f(\frac{\pi k}{W})$ where $k \in \mathbb{Z}$ assumes every integer value

$$f_W(t) = \sum_{k=-\infty}^{\infty} f\left(\frac{\pi k}{W}\right)\ \mathrm{sinc}(Wt - \pi k). \tag{2.9}$$

The sinus cardinalis $\mathrm{sinc}(t) = \sin(t)/t$ also appears in the context of the impulse response of an ideal band-pass filter.

The sampling theorem can be understood qualitatively in a very intuitive way. Consider a function with a very high band limit. This means that it shows modes with highly oscillatory behaviour. As a consequence any accurate discretization of the function must have short-distance samples.

Errors There are various sources of errors that appear in the context of the sampling theorem. Important for simulations are primarily the amplitude error, the truncation error and the aliasing error.

Errors in the value of the samples lead to so called amplitude errors. The round-off error may be considered a special case. This applies to all numerical computations due to the limited machine precision. The amplitude error is not discussed here any further. An outline on this topic can be found in [8].

The truncation error is a consequence of using only a finite set of samples when an infinite number is required. In practice this is relevant for calculations on grids

of finite extent with a nonvanishing function outside. The truncation error for the partial sum f_N with only $2N+1$ terms is

$$\begin{aligned}\mathcal{E}_T(t) &\equiv f(t) - f_N(t) \\ &= \sum_{|k|>N} f\left(\frac{k\pi}{W}\right) \frac{\sin(Wt - k\pi)}{Wt - k\pi}.\end{aligned} \tag{2.10}$$

Several estimates are covered again by [8].

Coming now to the source of error which will be given the most attention througout this document. The aliasing error $\mathcal{E}_A$ is the result of a sampling rate Δt^{-1} which underestimates the band-limit W of the signal

$$\frac{\pi}{\Delta t} < W. \tag{2.11}$$

The reconstruction Eq. (2.9) then acts as an ideal band-pass filter which cuts off all modes $|\omega| > \Omega$ with an absolute value greater than the assumed band-limit $\Omega = \pi/\Delta t$. The aliasing error of a band-restricted function f_Ω depends only on the spectral density outside the Nyquist range $[-\Omega,\Omega]$. It can be estimated to be below [10]

$$\begin{aligned}\mathcal{E}_A\left[f,\Omega\right](t) &\equiv |f(t) - f_\Omega(t)| \\ &\leq \frac{1}{\pi}\int_{|\omega|>\Omega} |\mathcal{F}(\omega)|\, d\omega.\end{aligned} \tag{2.12}$$

The above estimate is very good for almost all values of t except for those where $t = k\Delta t$ is a sampling point.

Relevance in quantum mechanics In quantum mechanics energy and momentum are related to time and space by Fourier transforms

$$\Psi(x,t) = \frac{1}{\sqrt{2\pi\hbar}} \int_{-p_{\max}}^{p_{\max}} \Psi(p,t)\, \exp(\tfrac{i}{\hbar}px)\, dp \tag{2.13a}$$

$$= \int_{-E_{\max}}^{E_{\max}} \Psi(x,E)\, \exp(-\tfrac{i}{\hbar}Et)\, dE. \tag{2.13b}$$

Note that the first representation corresponds to a decomposition into momentum eigenstates $\exp(\frac{i}{\hbar}px)$ with coefficients $\Psi(p,t) = \langle p \mid \Psi(t)\rangle$. The exponential in the energy representation on the other hand is a consequence of the Schrödinger time evolution as in Eq. (2.4) for a time-independent Hamiltonian. This also corresponds to an eigenstate decomposition with eigenfunctions $|E\rangle$ and $\Psi(x,E) = \langle x \mid E\rangle \langle E \mid \Psi(0)\rangle$.

This implies that for numerical quantum-mechanical computations of wave functions $\Psi(x,t)$ the sampling theorem explains fundamental limits for the timestep Δt and grid spacing Δx

$$\Delta t < \frac{\hbar\pi}{E_{\max}}, \qquad\qquad \Delta x < \frac{\hbar\pi}{p_{\max}}, \tag{2.14}$$

where $E_{\max}$ and $p_{\max}$ are the band-limits in the energy and momentum domain.

For general wave functions, however, energy and momentum may become arbitrarily large or may even be unlimited at all. Consequently the quantities Δx and Δt, which would be required for a correct representation, become unaffordably small.

A choice of Δx and Δt on the other hand which violates the requirements from Eq. (2.14) will lead to aliasing errors. To restrain aliasing errors the timestep and grid spacing can be chosen such that the spectral energy and momentum components higher than $\widetilde{E} = \hbar\pi/\Delta t$ and $\widetilde{p} = \hbar\pi/\Delta x$ become reasonably small.

Further error reduction may be achieved by a transformation of the considered wave-function such that the energy and momentum spectra become more centered around zero. This is discussed in more detail in Chapter 3.2.

2.3 Canonical transformations

Canonical transformations are mappings

$$|\Psi'\rangle = \hat{U}\,|\Psi\rangle\,, \tag{2.15a}$$

$$\hat{O}' = \hat{U}\hat{O}\hat{U}^\dagger \tag{2.15b}$$

of wave functions $|\Psi\rangle \in \mathcal{H}$ and hermitian operators $\hat{O} : \mathcal{H} \to \mathcal{H}$ to a transformed Hilbert space $\mathcal{H}'$ induced by a unitary operator $\hat{U}$. They preserve the canonical commutation relation of position and momentum operators $\hat{\boldsymbol{x}}$, $\hat{\boldsymbol{p}}$

$$\begin{aligned}\left[\hat{\boldsymbol{x}}', \hat{\boldsymbol{p}}'\right] &= \hat{U}\left[\hat{\boldsymbol{x}}, \hat{\boldsymbol{p}}\right]\hat{U}^\dagger = i\hbar \\ &= \left[\hat{\boldsymbol{x}}, \hat{\boldsymbol{p}}\right].\end{aligned} \tag{2.16}$$

Due to the unitarity of $\hat{U}$ expectation values remain constant and eigenvalue spetra are conserved

$$\begin{aligned}\langle\hat{O}'\rangle_{\Psi'} &= \langle\hat{U}\Psi \mid \hat{U}\hat{O}\hat{U}^\dagger \mid \hat{U}\Psi\rangle \\ &= \langle\hat{O}\rangle_{\Psi}\,,\end{aligned} \tag{2.17a}$$

$$\begin{aligned}\hat{O}'\,|o'\rangle &= \hat{U}\hat{O}\hat{U}^\dagger\hat{U}\,|o\rangle = \hat{U}o\,|o\rangle \\ &= o\,|o'\rangle\,.\end{aligned} \tag{2.17b}$$

This means that $\hat{O}$ and $\hat{O}'$ represent the same observable in different Hilbert spaces. Specifically we can see that if $|\Psi(t)\rangle$ fulfills the Schrödinger equation Eq. (2.1) then $|\Psi'(t)\rangle$ is a solution of a transformed Schrödinger equation

$$\hat{U}\left(i\hbar\frac{\partial}{\partial t}\right)\hat{U}^\dagger\,|\Psi'(t)\rangle = \hat{U}\hat{H}\hat{U}^\dagger\,|\Psi'(t)\rangle\,. \tag{2.18}$$

We can rearrange Eq. (2.18) to see that $|\Psi'(t)\rangle$ is also a solution of the Schrödinger equation in the original Hilbert space $\mathcal{H}$ with a transformed Hamiltonian $\hat{H}_{\hat{U}}$.

$$\begin{aligned} i\hbar\frac{\partial}{\partial t}|\Psi'(t)\rangle &= \left(\hat{U}\hat{H}\hat{U}^\dagger - \hat{U}i\hbar\frac{\partial\hat{U}^\dagger}{\partial t}\right)|\Psi'(t)\rangle \\ &\equiv \hat{H}_{\hat{U}}\,|\Psi'(t)\rangle\,. \end{aligned} \tag{2.19}$$

For the transformed wave function $|\Psi'\rangle$ expectation values of hermitian operators on the original Hilbert space $\mathcal{H}$ change according to

$$O' \equiv \langle\hat{O}\rangle_{\Psi'} = \langle\hat{U}^\dagger\hat{O}\hat{U}\rangle_{\Psi}\,. \tag{2.20}$$

For energy and momentum expectation values in particular this means a shift

$$E' = E + i\hbar\,\langle\hat{U}^\dagger(\partial_t\hat{U})\rangle_\Psi\,, \tag{2.21a}$$

$$\boldsymbol{p}' = \boldsymbol{p} - i\hbar\,\langle\hat{U}^\dagger(\partial_{\boldsymbol{x}}\hat{U})\rangle_\Psi\,. \tag{2.21b}$$

2.4 Gauge transformations

As a special type of canonical transformations, gauge transformations $\hat{U}$ are phase transformations induced by a real function $g(\boldsymbol{x},t)$

$$\langle\boldsymbol{x}\mid\hat{U}\Psi(t)\rangle \equiv e^{ig(\boldsymbol{x},t)}\,\langle\boldsymbol{x}\mid\Psi(t)\rangle\,. \tag{2.22}$$

This type of transformation conserves the probability density $|\Psi(\boldsymbol{x},t)|^2$. Furthermore, gauge transformations preserve the form of the Hamiltonian in Eq. (2.5) up to a change in the potentials

$$\hat{H}_{\hat{U}}(\hat{\phi},\hat{\boldsymbol{A}}) = \hat{H}(\hat{\phi}',\hat{\boldsymbol{A}}') \tag{2.23}$$

with transformed potentials

$$\boldsymbol{A}' = \boldsymbol{A} + \frac{\hbar c}{q}\,\frac{\partial g}{\partial\boldsymbol{x}}, \tag{2.24a}$$

$$\phi' = \phi - \frac{\hbar}{q}\,\frac{\partial g}{\partial t}. \tag{2.24b}$$

The electromagnetic fields are known to be invariant under gauge transformations

$$\begin{aligned} \boldsymbol{E}' &= -\partial_{\boldsymbol{x}}\phi' - \tfrac{1}{c}\partial_t\boldsymbol{A}' \\ &= -\partial_{\boldsymbol{x}}\phi + \tfrac{\hbar}{q}\partial_{\boldsymbol{x}}\partial_t g - \partial_t\boldsymbol{A} - \tfrac{\hbar}{q}\partial_t\partial_{\boldsymbol{x}}g \\ &= -\partial_{\boldsymbol{x}}\phi - \partial_t\boldsymbol{A} = \boldsymbol{E}, \end{aligned} \tag{2.25a}$$

$$\begin{aligned} \boldsymbol{B}' &= \partial_{\boldsymbol{x}}\times\boldsymbol{A}' \\ &= \partial_{\boldsymbol{x}}\times\boldsymbol{A} + \tfrac{\hbar c}{q}\partial_{\boldsymbol{x}}\times\partial_{\boldsymbol{x}}g \\ &= \partial_{\boldsymbol{x}}\times\boldsymbol{A} = \boldsymbol{B}. \end{aligned} \tag{2.25b}$$

According to Eqs. (2.21) energy and momentum are shifted by the gauge

$$E' = E - \hbar \langle (\partial_t g) \rangle \,, \tag{2.26a}$$

$$\boldsymbol{p}' = \boldsymbol{p} + \hbar \langle (\partial_{\boldsymbol{x}} g) \rangle \,. \tag{2.26b}$$

Note that it is irrelevant whether to take the transformed or the untransformed wave function for the spatial averaging in Eqs. (2.26). This means that energy and momentum in either representation can easily be measured from both systems.

3 Numerical integration of the Schrödinger equation

3.1 Integration schemes

Euler integration A naive approach to solve the Schrödinger equation (2.1) numerically is based on the temporal discretization

$$i\hbar\frac{\Psi_{n+1}-\Psi_n}{\Delta t} \doteq \hat{H}\Psi_n \tag{3.1}$$

which is equivalent to expanding the exponential in Eq. (2.3) to linear order

$$\Psi_{n+1} \doteq \left(1-\frac{i}{\hbar}\hat{H}\Delta t\right)\Psi_n. \tag{3.2}$$

However, this approximation is non-unitary and turns out to be unstable [11]. The exponential can be expanded to higher order to improve the error scaling. All finite expansions are of course non-unitary again, which is undesirable.

Crank-Nicolson An improvement is the Crank-Nicolson scheme [12]. It is based on the approximation of the exponential in Eq. (2.3) by the Cayley-form

$$\exp\left(-\frac{i}{\hbar}\hat{H}\Delta t\right) = \frac{1-i\hat{H}\Delta t/2\hbar}{1+i\hat{H}\Delta t/2\hbar} + \mathcal{O}\left((\hat{H}\Delta t)^3\right). \tag{3.3}$$

This is not only second order accurate – but also unitary and unconditionally stable. For one-dimensional problems the spatial matrix represenation of $1+i\hat{H}\Delta t/2\hbar$ has a simple band structure. That is if the momentum operator in the Hamiltonian is approximated using finite differencing of course. For a low-order finite differencing approximation it can therefore easily be inverted. A demonstration of this is given by Goldberg et al. [13].

Van Dijk and Toyama [14] show how the scheme can be generalized for higher order accuracy. The spatial accuracy can be controlled by the finite-differencing scheme of the momentum operator in the Hamiltonian. For the improvement of the time-advance they use higher order polynomials to approximate the propagating exponential.

Of course, there is a large variety of further integration schemes with individual strengths and areas of applicability [2].

3.2 Spectrum-guided-integration

Spectrum-guided-integration is a gauge-technique to reduce the limitations due to the sampling theorem. It was proposed by Bauke and Keitel [4].

As explained in Chapter 2.2 there is an upper bound for mesh spacing Δx in quantum mechanical computations induced by the band limit in the momentum domain. Wave functions with high mean momentum but narrow momentum spectrum are therefore suboptimal for numerical propagation. A gauge-transformation, however, may shift the momentum as demonstrated in Eq. (2.26). The same holds true for the timestep Δt and its limitation by the energy band limit of course.

The idea of spectrum-guided-integration is to center energy and momentum spectra approximately around zero by means of a gauge transformation and evaluate the time evolution in the transformed system. Since energy and momentum correspond to temporal and spatial derivatives, the transformation can reduce temporal and spatial oscillations. In the new gauge a larger timestep and mesh spacing may lead a numerical error of the same magnitude.

Reducing temporal oscillations For a real function $\overline{E}(t)$ consider the gauge function

$$g_{\overline{E}}(\boldsymbol{x}, t) = \frac{1}{\hbar} \int_0^t \overline{E}(\tau)\, d\tau. \tag{3.4}$$

The transformed potentials in Eq. (2.24) are as follows

$$\boldsymbol{A}'(\boldsymbol{x}, t) = \boldsymbol{A}(\boldsymbol{x}, t), \tag{3.5a}$$
$$\phi'(\boldsymbol{x}, t) = \phi(\boldsymbol{x}, t) - \tfrac{1}{q}\overline{E}(t). \tag{3.5b}$$

Since $g_{\overline{E}}$ is $\boldsymbol{x}$-independent only the energy expectation value in Eq. (2.26) changes while the momentum remains unaltered

$$E'(t) = E(t) - \overline{E}(t), \tag{3.6a}$$
$$\boldsymbol{p}'(t) = \boldsymbol{p}(t). \tag{3.6b}$$

For a good choice of $\overline{E}(t) \approx E(t)$ the new energy expectation value will approximately vanish thus reducing the band limit and temporal oscillations.

Reducing spatial oscillations A similar approach can be sought in order to reduce spatial oscillations. For a real function $\overline{\boldsymbol{x}}(t)$ let

$$\begin{aligned} g_{\overline{\boldsymbol{x}}}(\boldsymbol{x}, t) = \frac{1}{\hbar} \int_0^t d\tau \;\; & \overline{\boldsymbol{x}}(\tau) \cdot \frac{d}{d\tau} \left(m\dot{\overline{\boldsymbol{x}}}(\tau) + \tfrac{q}{c}\boldsymbol{A}(\overline{\boldsymbol{x}}(\tau), \tau) \right) \\ & - \frac{1}{\hbar}\, \boldsymbol{x} \cdot \left(m\dot{\overline{\boldsymbol{x}}}(t) + \tfrac{q}{c}\boldsymbol{A}(\overline{\boldsymbol{x}}(t), t) \right). \end{aligned} \tag{3.7}$$

The potentials from Eq. (2.24) become

$$\boldsymbol{A}'(\boldsymbol{x},t) = \boldsymbol{A}(\boldsymbol{x},t) - \boldsymbol{A}(\overline{\boldsymbol{x}}(t),t) - \tfrac{mc}{q}\,\dot{\overline{\boldsymbol{x}}}(t), \tag{3.8a}$$

$$\phi'(\boldsymbol{x},t) = \phi(\boldsymbol{x},t) - (\boldsymbol{x}-\overline{\boldsymbol{x}}(t))\cdot\frac{d}{dt}\left(\tfrac{m}{q}\,\dot{\overline{\boldsymbol{x}}}(t) + \tfrac{1}{c}\boldsymbol{A}(\overline{\boldsymbol{x}}(t),t)\right). \tag{3.8b}$$

In this gauge the expectation values for energy and momentum shift as

$$E'(t) = E(t) + (\langle\boldsymbol{x}\rangle(t) - \overline{\boldsymbol{x}}(t))\cdot\frac{d}{dt}\left(m\dot{\overline{\boldsymbol{x}}}(t) + \tfrac{q}{c}\boldsymbol{A}(\overline{\boldsymbol{x}}(t),t)\right), \tag{3.9a}$$

$$\begin{aligned}\boldsymbol{p}'(t) &= \boldsymbol{p}(t) - \left(m\dot{\overline{\boldsymbol{x}}}(t) + \tfrac{q}{c}\boldsymbol{A}(\overline{\boldsymbol{x}}(t),t)\right)\\ &= m\frac{d}{dt}\Big(\langle\boldsymbol{x}\rangle(t) - \overline{\boldsymbol{x}}(t)\Big) + \tfrac{q}{c}\left(\langle\boldsymbol{A}\rangle(t) - \boldsymbol{A}(\overline{\boldsymbol{x}}(t),t)\right).\end{aligned} \tag{3.9b}$$

In case of $\overline{\boldsymbol{x}}(t) \approx \langle\boldsymbol{x}\rangle(t)$ and $\boldsymbol{A}(\overline{\boldsymbol{x}}(t),t) \approx \langle\boldsymbol{A}\rangle(t)$ the energy shift becomes insignificant and the momentum will be centered approximately around zero.

Reducing both temporal and spatial oscillations Both of these shifts can simply be combined by taking a gauge function

$$g_{\overline{E},\,\overline{\boldsymbol{x}}} = g_{\overline{E}} + g_{\overline{\boldsymbol{x}}}. \tag{3.10}$$

The theoretical basis for spectrum-guided-integration being established there are still questions that remain. This thesis focusses on the error improvement in the spectrum-guided-integration gauge and on how to determine reasonable choices of the gauge-parameter functions $\overline{E}$ and $\overline{\boldsymbol{x}}$. Bauke and Keitel [4] proposed to use the classical energy and trajectory for these. They also stated that this is not suitable in all cases. For example there are problems without classical analogon or solution. Furthermore, the classical trajectory may significantly deviate from the quantum-mechanical one. Another possibility is that the wave consists of more than one wave packages in either momentum or configuration space. In all of these cases the resulting gauge is suboptimal.

3.3 Piecewise spectrum-guided-integration

For systems where the center-of-mass motion is unknown a priori, spectrum-guided-integration can still be applied heuristically. This can be implemented by continuously adapting the gauge in a way such that energy and momentum band limits are decreased for some time. In this context, it is suggestive to think about feedback systems, such as proportional–integral–derivative (PID) controlled heuristics, for the functions $\overline{x}$ and $\overline{E}$.

Another approach is to use successive retransformations. This enables to use the most simple heuristics for the parameter functions $\overline{E}$ and $\overline{\boldsymbol{x}}$. If the particle is not accelerated too much, its momentum and energy are approximately constant during

the interval $t_j \leq t \leq t_k$. Using the current energy $E(t_j)$, center-of-mass $\boldsymbol{x}(t_j)$ and its velocity $\boldsymbol{v}(t_j)$ to apply the gauge $g_j \equiv g_{\overline{E}_j, \overline{\boldsymbol{x}}_j}$ from Eq. (3.10) with

$$\overline{E}_j(t) = E(t_j), \tag{3.11a}$$
$$\overline{\boldsymbol{x}}_j(t) = \boldsymbol{x}(t_j) + (t - t_j)\, \boldsymbol{v}(t_j) \tag{3.11b}$$

yields a transformed wave function

$$|\Psi'(t)\rangle \equiv e^{ig_j(t)} \, |\Psi(t)\rangle \, . \tag{3.12}$$

Compared to the original wave function Ψ the transformed wave function Ψ' may show reduced oscillatory behaviour while the constancy-assumption holds true. In a computational framework the required quantities can be measured at any time t as follows

$$E(t) = \langle \hat{H}(t) \rangle_{\Psi(t)} \, , \tag{3.13a}$$
$$m\boldsymbol{v}(t) = \langle \hat{\boldsymbol{p}} - \tfrac{q}{c}\hat{\boldsymbol{A}}(t) \rangle_{\Psi(t)} \, , \tag{3.13b}$$
$$\boldsymbol{x}(t) = \langle \hat{\boldsymbol{x}} \rangle_{\Psi(t)} \, . \tag{3.13c}$$

When the constancy assumption ceases to be valid at the time t_j the system should be regauged. This can be achieved using Eqs. (3.13) within the transformed system $\hat{H}'$, $\hat{\boldsymbol{A}}'$ and $|\Psi'\rangle$ to determine $\overline{E}'_k$ and $\overline{\boldsymbol{x}}_k$. The new gauge has to be applied additionally to the existent gauge. Technically this means that the function g'_k has to be added to g_j and the wave function has to be multiplied by $\exp(ig'_k)$.

For implementational simplicity however, it may be more convenient to invert the present gauge after each gauge interval before immediately applying a new one. This can be implemented by determining the quantities from Eq. (3.13) for $\overline{E}_k$ and $\overline{\boldsymbol{x}}_k$ in the context of the original system, resetting the gauge function to g_k and multiplying the wave function by $\exp(i\Delta g) = \exp(i(g_k - g_j))$. Note that $\boldsymbol{x}(t)$, $\boldsymbol{v}(t)$ are mathematically invariant under gauge transformations and $E(t) = E'(t) + \hbar \, \langle (\partial_t g) \rangle_{\Psi'}$ can also be measured in the transformed system. Therefore there is no need to invert the present gauge for a measurement of these quantities. In fact a measurement of energy and momentum in the original system is likely to yield tainted results due to the cut-off in the Fourier spaces and should not be performed in praxis.

It should be mentioned that the two approaches are not equivalent for general vector potentials $\boldsymbol{A}$. In other words $g'_k + g_j \not\equiv g_k$. For a constant vector potential $\boldsymbol{A}(\boldsymbol{x}, t) = \boldsymbol{A}$ in contrast both techniques give the same results. A vector potential of this type implies drastical simplifications to the gauge functions Eqs. (3.4) and (3.7)

$$\begin{aligned} \hbar \, g_{\overline{E}_j}(\boldsymbol{x}, t) &= t\overline{E}_j \\ &= tE(t_j), \end{aligned} \tag{3.14a}$$
$$\begin{aligned} \hbar \, g_{\overline{\boldsymbol{x}}_j}(\boldsymbol{x}, t) &= -\boldsymbol{x} \cdot \left(m\dot{\overline{\boldsymbol{x}}}_j + \tfrac{q}{c}\boldsymbol{A} \right) \\ &= -\boldsymbol{x} \cdot \boldsymbol{p}(t_j). \end{aligned} \tag{3.14b}$$

In this case the gauge functions are linear functions of only time ($g_{\overline{E}}$) or space ($g_{\overline{\boldsymbol{x}}}$) respectively. Furthermore, their notion depends only on two constant quantities. These are the energy E_j and momentum $\boldsymbol{p}_j$. The transformed potentials are

$$\boldsymbol{A}'(\boldsymbol{x},t) = -\tfrac{mc}{q}\,\boldsymbol{p}_j, \tag{3.15a}$$

$$\phi'(\boldsymbol{x},t) = \phi(\boldsymbol{x},t) - \tfrac{1}{q}E_j. \tag{3.15b}$$

Note that the transformed vector potential $\boldsymbol{A}'$ is constant again. Under these simplified circumstances the reconfiguration from g_j to g_k can be performed in a single step using the energy E'_k and canonic momentum $\boldsymbol{p}'_k$ as in Eq. (2.26)

$$\hbar\,\Delta g_{\overline{E}} = t(E_k - E_j) = tE'_k, \tag{3.16a}$$

$$\hbar\,\Delta g_{\overline{\boldsymbol{x}}} = -\boldsymbol{x}\cdot m\,(\boldsymbol{v}_k - \boldsymbol{v}_j) = -\boldsymbol{x}\cdot\boldsymbol{p}'_k. \tag{3.16b}$$

The effect of this gauge transformation $\hat{U} = \exp(ig_{\overline{E},\overline{\boldsymbol{x}}})$ with $\overline{E}$ and $\overline{\boldsymbol{x}}$ as in Eqs. (3.14) on the Fourier representations (2.13) can be calculated. The momentum wave function transforms as

$$\begin{aligned}\Psi'(\boldsymbol{p},t) &= \int \Psi'(\boldsymbol{x},t)\,e^{-\frac{i}{\hbar}\boldsymbol{p}\boldsymbol{x}}\,d^3x \\ &= \int \Psi(\boldsymbol{x},t)\,e^{-\frac{i}{\hbar}(\boldsymbol{p}+\boldsymbol{p}_j)\boldsymbol{x}}\,e^{\frac{i}{\hbar}E_j t}\,d^3x \\ &= \Psi(\boldsymbol{p}+\boldsymbol{p}_j,t)\,e^{\frac{i}{\hbar}E_j t}\end{aligned} \tag{3.17a}$$

This means that the momentum is simply shifted by its expectation value at the time t_j. Analogously the energy representation is

$$\Psi'(\boldsymbol{x},E) = \Psi(\boldsymbol{x},E+E_j)\,e^{-\frac{i}{\hbar}\boldsymbol{p}_j\boldsymbol{x}} \tag{3.17b}$$

In fact this is not entirely restricted to the case of the piecewise spectrum-guided-integration with a constant vector potential. More generally, the effect of any spectrum-guided-integration (3.10) on the momentum distribution is only a shift. This is because $g_{\overline{E}}$ is $\boldsymbol{x}$-independent and $g_{\overline{\boldsymbol{x}}}$ is always the sum of an $\boldsymbol{x}$-independent term and a term which is linear in $\boldsymbol{x}$, see Eqs. (3.4) and (3.7).

3.4 Generalizations to the spectrum-guided-integration

As previously explained the general idea of the spectrum-guided-integration is to reduce temporal and/or spatial oscillations in the regions of high density $|\Psi(\boldsymbol{x},t)|^2$. Unfortunately its effective application is restricted to wave functions with a single narrow momentum or energy band. Furthermore, the reduction of spatial oscillations depends on a well-behaving vector potential. Highly accelerated systems with unknown center-of-mass motion pose additional problems.

To overcome some of the difficulties of the spatial spectrum-guided-integration, the technique can be generalized to work for cases where the phase differences between individual space-points do not grow very fast.

Zero-phase gauge In principle there is always a gauge for which the (spatial) phase oscillations vanish completely. This is obvious, considering

$$\Psi(\boldsymbol{x},t) = e^{ig(\boldsymbol{x},t)}|\Psi(\boldsymbol{x},t)|, \tag{3.18}$$

where

$$g(\boldsymbol{x},t) = \arg(\Psi(\boldsymbol{x},t)). \tag{3.19}$$

Using $-g(\boldsymbol{x},t)$ as gauge function, a wave function Ψ' is obtained. From $\Psi'(\boldsymbol{x},t) = |\Psi'(\boldsymbol{x},t)|$, it follows immediately that

$$\begin{aligned}\langle\hat{\boldsymbol{p}}\rangle_{\Psi'(t)} &= \int \Psi'(\boldsymbol{x},t)(-i\hbar)\frac{\partial\Psi'(\boldsymbol{x},t)}{\partial\boldsymbol{x}}\,d^3x \\ &= -\int \frac{\partial\Psi'(\boldsymbol{x},t)}{\partial\boldsymbol{x}}(-i\hbar)\Psi'(\boldsymbol{x},t)\,d^3x = 0.\end{aligned} \tag{3.20}$$

The second equality is obtained by partial integration. This means that the zero-phase gauge leads to a vanishing mean momentum, just like the optimal spectrum-guided-integration.

Consider a discretized wave function Ψ. For the spatial domain the referred gauge can easily be found at any timestep by measuring the phase $\arg(\Psi(\boldsymbol{x},t))$ at each grid point and interpolating a function $g(\boldsymbol{x})$. Of course, care must be taken to avoid 2π phase jumps. A multiplication of the wave function by $\exp(-ig(\boldsymbol{x}))$ sets the phase to zero everywhere. As this aims to reduce only spatial oscillations, the same gauge function $g(\boldsymbol{x})$ is used for a few time steps, until the system needs regauging. The scalar function g is then time-independent. The derivatives $\partial_{\boldsymbol{x}}g(\boldsymbol{x})$ at each point, which are needed for the transformed vector potential $\boldsymbol{A}'$, can be calculated by finite differencing.

Actually this approach should not be considered too closely related to the spectrum-guided-integration. The spectrum-guided-integration seeks to lessen phase oscillations by shifting the wave function in momentum space and reducing its band limit. Here in constrast only the phase of wave function is set to the same value everywhere at one instant. As opposed to the spectrum-guided-integration the effect of the transform goes far beyond a shift in the momentum spectrum. The momentum wave function may be completely deformed, as the gauge function is in general not linear in $\boldsymbol{x}$. The deformation can compress the momentum distribution, which is a good thing. Unfortunately, there is also the possibility that the momentum distribution is spread or even split.

Moreover temporal variations are not taken into account at all. This means that even if the assumed gauge is optimal at one instant, it might become completely useless soon after. There are no obvious means to ensure the durability of the zero-phase-gauge.

Furthermore, the phase and derivatives thereof are of order unity everywhere. Strictly interpolating a phase function can thus introduce highly $\boldsymbol{x}$-dependent behaviour of the vector-potential. Even for regions where the density is so low that every measurable phase oscillation is essentially only numerical noise.

Phase fit gauge The latter problem can be solved by replacing the interpolation by an approximation method. Curve approximations can be implemented by using some kind of fit. The weights of the fit should scale with the density of the wave function. This prevents from installing unphysical $\boldsymbol{x}$-dependency of the gauge function in areas of little interest.

By the choice of the fitting function, it can also be specified how the shape of the momentum distribution changes due to the transformation. A linear fit for example corresponds to the piecewise spectrum-guided-integration. For general fit functions however the effect on the momentum spectrum is hard to work out.

In this work a B-spline fit is used to test for the feasibility of this idea in principle. B-splines provide the possibility of piecewisely smooth polynomial interpolation or approximation of large datasets. Globally smooth approximations tend to be prone to the Runge phenomenon, which means that they show oscillations at the edges of the domain of definition. To prevent this, the x-axis is broken up into a number of intervals when fitting with B-splines. The endpoints of each interval are called *breakpoints*. At the breakpoints, the smoothness conditions are allowed to be less rigid, which allows to avoid the Runge phenomenon. The usage of a B-splines fit allows for non-targeted usage, since phase-functions of arbitrary shape can be approximated. Further information is available in [15].

Note that this approach is compatible with the temporal variant of the spectrum-guided-integration. This means that a gauge can be obtained which reduces both spatial and temporal oscillations, by just adding

$$g(\boldsymbol{x}, t) = g_{\text{fit}}(\boldsymbol{x}) + g_{\overline{E}}(t). \tag{3.21}$$

3.5 Error estimates for the spectrum-guided-integration

Consider a computation on a mesh of constant extent L with constant grid spacing Δx. Further assume that the error of the computation originates solely from an accumulation of the aliasing error $\mathcal{E}_A$ due to the momentum cut-off. In this case an estimate of the error can be made.

In the standard representation Ψ, the momentum expectation value is $\overline{p} \equiv \langle \hat{p} \rangle_\Psi$. Assume an optimal spectrum-guided-integration gauge Ψ'. That is $\overline{p}' \approx 0$. For comparison denote the maximum aliasing errors which effect from the individual representations $\epsilon_A \equiv \max\{\mathcal{E}_A[\Psi, \tilde{p}](x)\}$ and $\epsilon'_A \equiv \max\{\mathcal{E}_A[\Psi', \tilde{p}](x)\}$. For both setups the same grid spacing Δx and hence momentum cut-off $\tilde{p}$ is assumed. Using Eq. (2.12), it follows

$$\begin{aligned}
\epsilon'_A &\approx \frac{1}{\pi} \int_{|p|>\tilde{p}} |\Psi'(p)| \, dp \\
&= \frac{1}{\pi} \int_{|p+\overline{p}|>\tilde{p}} |\Psi(p)| \, dp \\
&= \epsilon_A + \frac{1}{\pi} - \frac{1}{\pi} \int_{\tilde{p}}^{\tilde{p}+\overline{p}} |\Psi(p)| \, dp.
\end{aligned} \tag{3.22}$$

The second line follows considering that the transformed momentum wave function $\Psi'(p)$ is merely shifted, see Eq. (3.17a). For high momenta $|\overline{p}|$ one of the integral terms in Eq. (3.22) can be neglected if the momentum wave function $\Psi(p)$ decays reasonably fast on deviations from the mean momentum. For example $0 < \overline{p} < \tilde{p}$, then

$$\epsilon'_A \approx \epsilon_A - \frac{1}{\pi} \int_{\tilde{p}}^{\tilde{p}+\overline{p}} |\Psi(p)|\, dp < \epsilon_A. \tag{3.23}$$

In case of $-\tilde{p} < \overline{p} < 0$, then

$$\epsilon'_A \approx \epsilon_A - \frac{1}{\pi} \int_{-\tilde{p}+\overline{p}}^{-\tilde{p}} |\Psi(p)|\, dp < \epsilon_A. \tag{3.24}$$

The resulting aliasing error is smaller than in the original gauge.

It is of additional interest how much the mesh spacing $\Delta x'$ can be increased over Δx without increasing the resulting maximum aliasing error. Assume Δx and $\Delta x'$ respectively are the spacings which lead to the same aliasing error $\epsilon_A = \epsilon'_A$. By Eq. (2.14) it follows

$$\frac{\Delta x'}{\Delta x} = \frac{\tilde{p}}{\tilde{p}'}\,, \tag{3.25}$$

where $\tilde{p}$ and $\tilde{p}'$ are the band limits which lead to the same aliasing error

$$\epsilon_A = \max\{\mathcal{E}_A[\,\Psi, \tilde{p}\,](x)\} \tag{3.26a}$$

$$= \max\{\mathcal{E}_A[\,\Psi', \tilde{p}'\,](x)\}. \tag{3.26b}$$

Remember that the aliasing error ϵ_A depends only on the spectral density outside the Nyquist range $[-\tilde{p}, \tilde{p}]$. Considering that the spectrum-guided-integration essentially only shifts the momentum distribution, a natural speculation is that the aliasing error will be about the same, when $\tilde{p} \approx |\overline{p}| + \tilde{p}$. Therefore it is suggestive to write $\tilde{p}$ as deviation from the momentum expectation value $\overline{p}$. Using the momentum variance $\sigma_p = \sigma'_p$ to rewrite $\tilde{p} = |\overline{p}| + K\sigma_p$ and $\tilde{p}' = K'\sigma_p$ in Eq. (3.25) gives

$$\begin{aligned} \frac{\Delta x'}{\Delta x} &= \frac{K\sigma_p + |\overline{p}|}{K'\sigma_p} \\ &= \frac{K}{K'} + \frac{|\overline{p}|}{K'\sigma_p}. \end{aligned} \tag{3.27}$$

If the momentum wave function does not vary its shape too much over the course of time, the values for K and K' are approximately constant. For momentum distributions $\Psi(p)$ which decay rapidly on deviation from the mean momentum $\overline{p}$, the ratio K/K' will be around unity. The ratio of mesh widths Δx, $\Delta x'$ giving the same aliasing error after an integration over the time T can be estimated with an easy expression

$$\begin{aligned} \frac{\Delta x'_T}{\Delta x_T} &\approx \frac{1}{T} \int_0^T dt\, \frac{\Delta x'}{\Delta x} \\ &\approx 1 + \frac{1}{T} \int_0^T dt\, \frac{|\overline{p}|}{K'\sigma_p}. \end{aligned} \tag{3.28}$$

The integral term is always larger than zero. This means that the grid spacing is always increased by spectrum-guided-integration. Furthermore, the amount of increase is dependent mainly on the mean ratio of the momentum expectation value and its spread $\overline{p}/\sigma_p$.

Considering the very limiting prerequisites and naive assumptions, this result is of course highly qualitative and can not easily be applied for general problems. Nontheless the main conclusions which were drawn from Eq. (3.28) should be valid in a larger variety of cases.

4 Numeric results

In this section, the integration strategies from Chapter 3 will be applied to a few one-dimensional model systems. The numerical simulations are carried out by C++ programs which rely on Heiko Bauke's Q-Wave software library. All calculations are performed in atomic units which implies $e = m_e = \hbar = 1$. A Crank-Nicolson scheme of forth order was adopted as integration scheme. The B-spline fits are implemented with help of the GNU Scientific Library [16].

4.1 The one-dimensional harmonic oscillator

As the first example a gaussian wave packet in a one-dimensional harmonic oscillator was considered. Further information on the harmonic oscillator can be found in introductory textbooks about quantum mechanics [6].

Note that the harmonic oscillator has a time-independent Hamiltonian and therefore a constant energy spectrum. Hence the piecewise energy-gauge $g_{\overline{E}}$ is rather uninteresting and needs no further discussion as there is basically no difference from the work of Bauke and Keitel [4]. The phase fit method is not expected to give any qualitative differences either – since there is only a single localized wave packet. Therefore, the only method about to be examined is the spatial piecewise spectrum-guided-integration.

Analytics In standard representation the Hamiltonian is

$$\hat{H} = \frac{1}{2m}\hat{p}^2 + \frac{m\omega^2}{2}\hat{x}^2. \tag{4.1}$$

This problem is known to be solvable analytically with energy-eigenstates $|n\rangle$ to the eigenvalues E_n, where

$$\langle x \mid n\rangle = \frac{1}{\sqrt{2^n n!}} \left(\frac{m\omega}{\pi\hbar}\right)^{\frac{1}{4}} H_n\left(\sqrt{\frac{m\omega}{\hbar}}\, x\right) \exp\left(-\frac{m\omega}{2\hbar}x^2\right), \tag{4.2a}$$

$$E_n = \left(n + \tfrac{1}{2}\right)\hbar\omega. \tag{4.2b}$$

The Hermite polynomials H_n are of degree n. An initial state $|\Psi(0)\rangle$ can be decomposed into eigenstates to calculate the exact time evolution

$$\begin{aligned} |\Psi(t)\rangle &= \exp\left(-\tfrac{i}{\hbar}\hat{H}t\right)|\Psi(0)\rangle \\ &= \sum_{n=0}^{\infty} \exp\left(-\tfrac{i}{\hbar}E_n t\right)|n\rangle\,\langle n \mid \Psi(0)\rangle\,. \end{aligned} \tag{4.3}$$

The first equality follows from the time-independence of the Hamiltonian. The second step is the consequence of the decomposition $|\Psi(0)\rangle = \sum_{n=0}^{\infty} |n\rangle \langle n \mid \Psi(0)\rangle$.

In the following computations a gaussian wave packet of width σ_x is chosen as the initial condition

$$\Psi(x,0) = \left(\frac{1}{2\pi\sigma_x^2}\right)^{\frac{1}{4}} \exp\left(\frac{(x-x_0)^2}{4\sigma_x^2} + \frac{i}{\hbar}p_0(x-x_0)\right). \tag{4.4}$$

As the gaussian wave packet has minimal uncertainty, initially $\sigma_x\sigma_p = \hbar/2$. An explicit expression for the exact solution is well known, see for example [17] and [18]. The center-of-mass motion for a gaussian wave packet in the harmonic oscillator follows the classical solution

$$x(t) = x_0\cos(\omega t) + \frac{p_0}{m\omega}\sin(\omega t). \tag{4.5}$$

Also the width of the wave packet oscillates as

$$\begin{aligned}\sigma_x^2(t) &= \sigma_x^2\cos^2(\omega t) + \frac{\sigma_p^2}{m^2\omega^2}\sin^2(\omega t)\\ &= \sigma_x^2 + \left(\frac{\sigma_p^2}{m^2\omega^2} - \sigma_x^2\right)\sin^2(\omega t)\end{aligned} \tag{4.6a}$$

and analogously

$$\sigma_p^2(t) = \sigma_p^2 + \left(m^2\omega^2\sigma_x^2 - \sigma_p^2\right)\sin^2(\omega t). \tag{4.6b}$$

An examination of the uncertainty variation for more general localized wave packets is done by Qiong-Gui Lin [19].

The initial state has the constant energy expectation value and variance

$$E = \frac{1}{2m}p^2 + \frac{m\omega^2}{2}\sigma_x^2 + \frac{\hbar^2}{8m\sigma_x^2}, \tag{4.7a}$$

$$\sigma_E^2 = \frac{m^2\omega^4}{2}\sigma_x^4 + \frac{\hbar^4}{32m^2\sigma_x^4} - \frac{\hbar^2\omega^2}{4} + \frac{\hbar^2p^2}{4m^2\sigma_x^2}. \tag{4.7b}$$

Choice of parameters and criteria for grid spacing and timestep As system characteristics $m = \omega = 1$ is chosen. The initial wave packet is described by $p_0 = 8$, $\sigma_x = 0.71$ and $x_0 = 0$. For this setup it follows from Eqs. (4.6) that the variation of the uncertainties σ_x, σ_p is small compared to their initial values. Explicitly

$$\frac{\sigma_x^2(t) - \sigma_x^2}{\sigma_x^2} \approx -0.0162 \cdot \sin^2(\omega t), \tag{4.8a}$$

$$\frac{\sigma_p^2(t) - \sigma_p^2}{\sigma_p^2} \approx +0.0165 \cdot \sin^2(\omega t). \tag{4.8b}$$

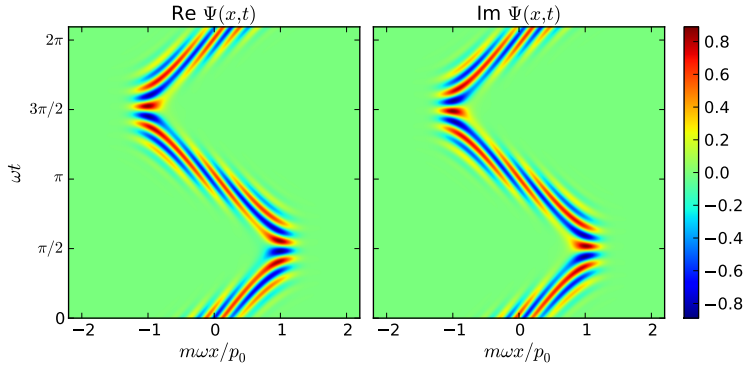

(a) Wave function in ordinary gauge

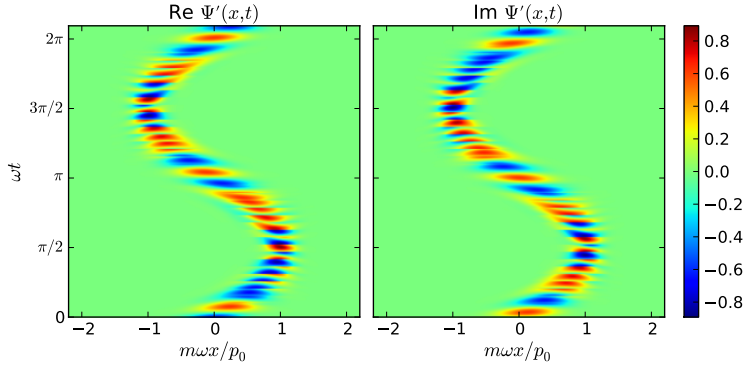

(b) Piecewisely transformed wave function

Figure 4.1: Real and imaginary part of wave functions $\Psi(x,t)$ in the ordinary gauge of the harmonic oscillator and $\Psi'(x,t)$ in the piecewise spectrum-guided-integration gauge. The initial state is a gaussian wave packet with $p_0 = 5$ and $\sigma_x = 1$.

The energy expectation value and variance from Eqs. (4.7) become

$$\frac{E}{\hbar\omega} \approx 32.5, \qquad \frac{\sigma_E}{\hbar\omega} \approx 5.6. \tag{4.9}$$

The spectral energy component at $E + 7\sigma_E$ drops to about 4.5×10^{-5} of the value at E. It should therefore be safe to assume $E_{\max} = E + 7\sigma_E$ for practical purposes. Considering the limit Eq. (2.14) the timestep must satisfy

$$\Delta t < \frac{\hbar\pi}{E_{\max}} \approx 0.044. \tag{4.10}$$

As the energy spectrum is time-invariant the criterion for the the timestep remains valid during the integration. The grid spacing Δx is restricted by the band limit in the momentum domain

$$\Delta x < \frac{\hbar\pi}{p_{\max}} \approx 0.27, \tag{4.11}$$

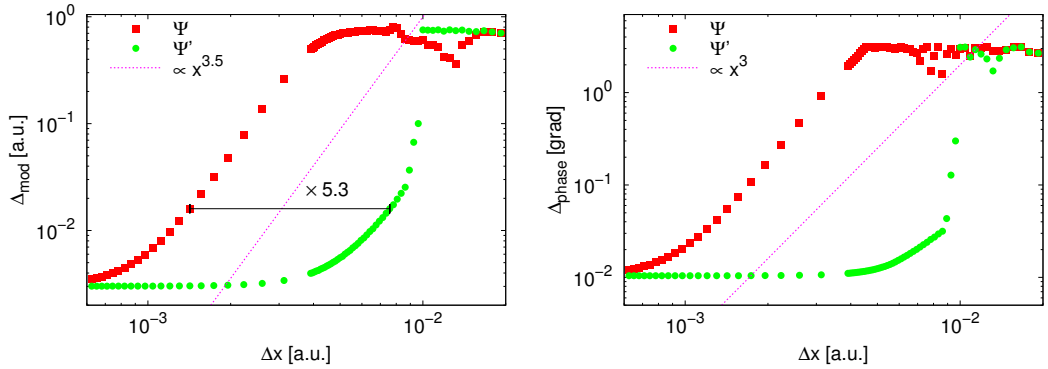

(a) Density error Δ_{mod} **(b)** Phase error Δ_{phase}

Figure 4.2: Errors of untransformed wave function $\Psi(x,t)$ and transformed wave function $\Psi'(x,t)$ as a function of grid spacing Δx. The initial state is a gaussian wave packet with $x_0 = 0$, $p_0 = 8$ and $\sigma_x = 0.71$.

where $p_{\max} = p + 7\sigma_p$ is assumed. Since the spectral momentum component at $p + 7\sigma_p$ is about 4.8×10^{-6} of the value at p, this can be considered a reasonable approximation. Note that the momentum is at its maximum initially which means that Eq. (4.11) never overestimates the required grid spacing.

With this choice of Δx the momentum aliasing error can be estimated according to Eq. (2.12) to be below

$$\mathcal{E}_A[\Psi, p_{\max}](x) \leq 1.7 \times 10^{-6} \tag{4.12}$$

which is good enough for demonstrational purposes.

Results Figure 4.1 illustrates the effect of the spectrum-guided-integration gauge. In the standard representation, see Fig. 4.1a, the system shows highly oscillatory behaviour in both time and space. The piecewise spectrum-guided-integration is capable of nearly eliminating the spatial oscillations for a short time, see Fig. 4.1b.

The regauging was always performed after the same number of integration steps. No heuristics were used to predict more adaptive intervals. The intervals used to produce Fig. 4.1 were rather large for demonstrational purposes. For shorter regauge intervals the image soon becomes indistinguishable from the result of the ordinary spectrum-guided-integration, as presented by Bauke and Keitel. This comes not unexpected, considering that the continuous limit of the gauge function is $g_{\overline{x}(t)}$, where $\overline{x}(t)$ is the classical trajectory.

A more quantitative impression of how much the spectrum-guided-integration allows to improve the accuracy is given in Figs. 4.2. Figure 4.2a shows the error

$$\Delta_{\mathrm{mod}} = \max\left\{\left|\,|\Psi_{\mathrm{ana}}(x,T)| - |\Psi_{\mathrm{num}}(x,T))|\,\right|\right\} \tag{4.13}$$

of the wave function absolute value after the integration time T. In the power law regime, the ratio of grid spacings for the same maximum error is about $\Delta x'/\Delta x \approx 5$. The phase error

$$\Delta_{\text{phase}} = \max\left\{\left|\arg(\Psi_{\text{num}}(x,T)/\Psi_{\text{ana}}(x,T))\right| : |\Psi_{\text{ana}}(x,T)|^2 > \rho_{\min}\right\} \tag{4.14}$$

is shown in Fig. 4.2b. The error is only evaluated at points where the probability density exceeds a minimum $\rho_{\min} = 0.1$. The purpose of this restriction is to prevent the curve to show minor numerical errors for points of small $|\Psi(x,T)|^2$ where the phase error can still be up to π. The phase-error graph losely confirms the previous result for the benefit factor $\Delta x'/\Delta x \approx 5$.

To reduce boundary effects, only x with reasonable distance from the edges were considered.

Checking the error estimate The analytic solution and knowledge about the physical properties of the harmonic oscillator can be used to check the error estimates from Chapter 3.5. First take a look at the prerequisites:

- The error is dictated by the specifics of the used integration algorithm. It is not the case, that the error results exclusively from an aliasing error, neither that the calculation depends on the Shannon sampling representation. Rather, the numerical integration introduces errors from an inexact solution of the underlying differential equation. These are not of the spatial aliasing error type. The timestep is chosen very small though, so this does not dominate the error.
- A gaussian wave packet is chosen as initial state. Therefore, the initial momentum distribution is also of gaussian form. This means that the momentum spectral density decays exponentially on deviations from the mean momentum. Then $K/K' \approx 1$ can be assumed.
- The chosen wave packet will not spread or concentrate much over time, even in the presence of the harmonic potential, see Eq. (4.8). Therefore, K,$K' \approx$ const is a reasonable assumption.

According to Eq. (3.28) the ratio $\Delta x'/\Delta x$ for the same error ϵ_A averaged over the hole integration time $T = 2\pi$ is

$$\frac{\Delta x'}{\Delta x} \approx 1 + \frac{1}{2\pi}\int_0^{2\pi} \frac{\langle\hat{p}\rangle}{K'\sigma_p}\, dt. \tag{4.15}$$

Note that $\epsilon_A = \|\Psi_{\text{ana}} - \Psi_{\text{num}}\|_\infty$ is closely related to, but not the same as the modulus error Δ_{mod}. With the classical trajectory $\langle\hat{p}\rangle = p_0\cos(\omega t)$ and $\sigma_p \approx$ const:

$$\begin{aligned}\frac{\Delta x'}{\Delta x} &\approx 1 + \frac{p_0}{2\pi K'\sigma_p}\int_0^{2\pi} |\cos(\omega t)|\, dt \\ &= 1 + \frac{2p_0}{\pi K'\sigma_p\omega} \\ &\approx 1 + \frac{2p_0\Delta x'}{\hbar\pi^2\omega}.\end{aligned} \tag{4.16}$$

This predicts a linear increase of the benefit with $\Delta x'$. In contrast the numerical result as in Fig. 4.2a show a ratio $\Delta x'/\Delta x$ which is approximately constant over a large scale. For $\Delta x' = 0.083$ the estimate Eq. (4.16) leads to an expected value $(\Delta x'/\Delta x)_{\text{expect}} \approx 1.1$. The numerical result is $(\Delta x'/\Delta x)_{\text{num}} \approx 5$.

This shows that the estimate from Eq. (3.28) is not applicable. It vastly underestimates the benefit due to the spectrum-guided-integration. In addition it gives an incorrect scaling prognosis.

This comes from the incorrectness of the assumption, that the total computational error is just a linear accumulation of the Shannon-sampling aliasing error.

The errors for $\Delta x \approx 5 \times 10^{-3}$ are of order one, which is about the maximum value of the probability density. We can see that Eq. (4.11) overestimates the maximum usable grid spacing by two orders of magnitude. This gives another indication that the algorithm specific stability criteria become important long before the fundamental limit due to the sampling theorem is reached.

Accuracy in terms of computation time For real world applications it is often of more interest how the error scales with computational time τ rather than memory usage $N \sim \Delta x^{-d}$, where d is the dimension and N is the total number of grid points.

The piecewise spectrum-guided-integration requires a momentum and center-of-mass measurement every M timesteps. Additionally a transformation of the wave function every M timesteps must be accounted for, as well as the evaluation of the transformed potentials at each timestep.

On the other hand some integration algorithms may converge faster using the transformed wave function. This can reduce the number of iterations and thus the total computational time.

Using the number of floating-point-operations as an indicator for the computational time, the additional steps can all be performed in $\mathcal{O}(N)$. It follows that the

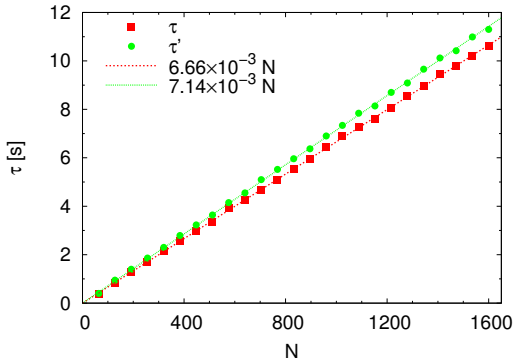

Figure 4.3: Corresponding computation times τ for standard harmonic oscillator and τ' with the piecewise spectrum guided integration. The initial parameters were $p = 8$, $m = \omega = 1$, $\sigma_x = 0.71$.

computational time per timestep increases as

$$\tau' = \tau + \mathcal{O}(N). \tag{4.17}$$

The additional costs due to the transformation should therefore be at most linear in the number of grid points.

This is confirmed by Fig. 4.3. The piecewise spectrum-guided-integration was on average slower by a factor of $\tau'/\tau \approx 1.1$ for the same $\Delta x(N)$. The computation time scales linear with $N \sim \Delta x^{-1}$. Hence, in terms of computational cost, the effective gain is described by

$$\frac{\tau'(\Delta x'(\epsilon))}{\tau(\Delta x(\epsilon))} = \frac{\Delta x(\epsilon)}{\Delta x'(\epsilon)} \cdot \frac{\tau'}{\tau} \approx 0.21. \tag{4.18}$$

This means that the benefit of using the spectrum-guided-integration outscales its additional cost by a factor of 4 to 5 in the examined case.

4.2 Ionization in a one-dimensional softcore potential

The developed gauge techniques shall now be applied in the simulation of a laser induced ionization process. Atoms or ions with a single electron can be described by Coulomb potentials

$$\phi(r) \sim r^{-1}. \tag{4.19}$$

The numerical description of Coulomb potentials is difficult due to the singularity at the origin. Therefore, a softcore potential can be taken as a more stable substitute for the Coulomb potential. Softcore potentials are very similar to Coulomb potentials but do not have the singularity. The form of a softcore potential is

$$\phi(\boldsymbol{x}) = \frac{Z}{\sqrt{(\boldsymbol{x} - \boldsymbol{x}_0)^2 + \zeta^2}}. \tag{4.20}$$

Setup The softcore potential is determined by the parameters $\zeta = \sqrt{2}$ and $Z = -1$. The system shall be modelled in dipole approximation. For simplified application of the piecewise constant spectrum-guided-integration, see Chapter 3.3, the laser is initially described in a gauge with vanishing vector potential. A linear ramp is used to turn the laser on and off. The laser stays at its full intensity for one half cycle. This means

$$\phi(\boldsymbol{x}, t) = \boldsymbol{x} \cdot \boldsymbol{E}_0 \ \sin(\omega t)\chi(\omega t), \tag{4.21a}$$

$$\boldsymbol{A}(\boldsymbol{x}, t) = 0 \tag{4.21b}$$

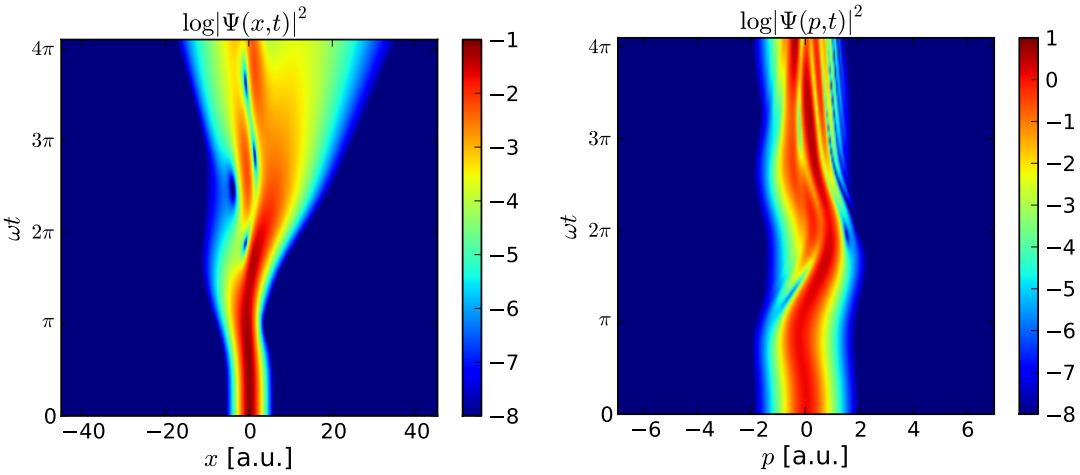

(a) Spatial representation

(b) Momentum representation

Figure 4.4: Time evolution of (a) spatial and (b) kinetic momentum probability density in the softcore potential with $\zeta = \sqrt{2}$, $Z = -1$. The laser wave length is $\lambda = 3000$, its field strength $E_0 = 0.12$. $N = 512$ grid points were used.

where $\omega = 2\pi/\lambda$ is the angular frequency of the laser, $\boldsymbol{E}_0$ its electric field vector and $\chi(\alpha)$ the turn-on/turn-off envelope

$$\chi(\pi\alpha) = \begin{cases} \alpha & 0 \leq \alpha \leq 1 \\ 1 & 1 \leq \alpha \leq 2 \\ 3 - \alpha & 2 \leq \alpha \leq 3 \\ 0 & \text{else.} \end{cases} \tag{4.22}$$

As the initial state, the ground state of the softcore potential is taken. The ground state with $E = -0.5$ was found numerically using imaginary time evolution [20, 21]. The parameters for the laser are taken as $\boldsymbol{E}_0 = 0.12$ and $\lambda = 3000$.

Results For this system all of the optimization strategies from Chapters 3.3 and 3.4 make sense, principally. The spatial spectrum-guided-integration and B-spline phase fit will be discussed in detail.

Figure 4.4 shows the time evolution of the system. Note that at $\omega t = 3\pi$ the Hamiltonian becomes time-independent. Therefore, the state at $\omega t = 3\pi$ already contains the final energy spectrum, which means that all unbound states are completely determined. The integration stops after $\omega t = 4\pi$ for demonstrational purposes. An escaping probability flux in the positive x domain can be clearly identified at this stage.

For error comparison, a numeric solution in the standard representation was obtained using a vastly higher number of grid points $N = 4095$. The results were then

interpolated to grids of smaller N with Shannon's reconstruction formula, as in Eq. (2.9). The expectations and results for the individual methods will now be discussed in detail.

Standard representation In the process of the ionization, eventually a portion of the wave function gains high momentum and leaves the central potential. This part is a superposition of unbound states. There are two obvious representational choices where either the momentum of the remaining bound states or the momentum of the escaping states vanishes.

In the case of vanishing bound state momentum, the unbound density flux has high momentum. Consequently the unbound part needs a more fine grained x-resolution than the bound portion of the particle. On the other hand, a transformation to a gauge where the momentum of the unbound portion vanishes, naturally introduces a high momentum for the bound states. This indicates that neither of these representations will yield optimal results.

The electromagnetic potentials from Eqs. (4.21) correspond of course to a vanishing bound-state momentum. Due to the vanishing vector-potential $\boldsymbol{A} = 0$ the kinetic momentum equals the canonic momentum. This representation is referred to as *standard gauge* and used as reference for comparisons.

Piecewise spectrum-guided-integration The spectrum-guided-integration allows somewhat of a compromise. We are not forced to make either the bound-state or the unbound-state momentum vanish. Rather, with this technique the mean momentum of all emerging wave packages can be shifted to zero. If the wave packages are too distinct in momentum space, however, the gauge is optimal for neither of them. This leads to the expectation that the spectrum-guided-integration approach will not

Figure 4.5: Time evolution of $\arg(\Psi)$ in the softcore potential with $\zeta = \sqrt{2}$, $Z = -1$. The laser wave length is $\lambda = 3000$, its field strength $E_0 = 0.12$. $N = 512$ grid points were used. The graphs correspond to (a) standard representation, (b) piecewise spectrum-guided-integration and (c) B-spline fit gauge

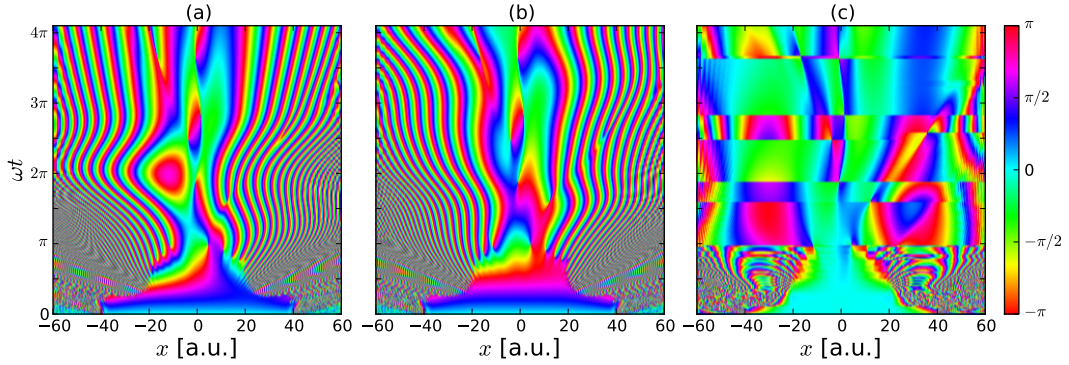

be significantly better than a description in the standard gauge.

In fact, Fig. 4.6a shows that the spatial spectrum-guided-integration gives worse results than the standard representation.

The reason for this is exhibited in Fig. 4.4b, which shows the momentum distribution in the standard representation. We can see that the mean momentum is small compared to its width. According to the qualitative estimate Eq. (3.28), this indicates that an application of the (spatial) spectrum-guided-integration will hardly give any error improvements. The phase-diagram Fig. 4.5 confirms this speculation. The graph shows explicitly, that the spectrum-guided-integration is unable to reduce phase oscillations in the case at hand.

The influence of the temporal variant of the piecewise spectrum-guided-integration was also examined. The numerics of all discussed spatial gauge-strategies were performed with and without using an additional $g_{\overline{E}}$ term. No significant differences for the errors were found. This is to be expected due to the lacking involvment of high energies.

Zero phase interpolation The description of two very distinct momentum wave packages clearly poses a problem for the piecewise spectrum-guided-integration as it can only shift the momentum distribution. The key to solving the dilemma may lie in the deformation of the momentum spectrum. For this, gauge-functions must be used which are non-linear in $\boldsymbol{x}$. This leads to the use of one of the generalizations discussed in Chapter 3.4.

Unfortunately any attempt to impose the zero-phase gauge was highly unstable. After a few timesteps numerical results were totally flawed and wave function values of up to infinity were obtained.

The reason for this could not be determined in detail. It can be speculated that the instabilities arise from the regidity of the phase interpolation in areas of low density. Here small variations in the wave function actual value can appear as major phase differences. The derivative of the gauge function and the transformed vector potential become then unreasonably large.

B-spline fit gauge It is possible to overcome the problem, which was speculated to be the reason for the instability of the zero-phase gauge. The minor importance of the low-density areas has to be taken into account. It is natural to implement this via a weighted fit, were the weights are monotonous functions of the density. Here, the weigths were set to be equal to the wave function density $|\Psi(x,t)|^2$. Quadratic B-splines with $N_{\text{break}} = 4$ breakpoints were used to perform the fit.

This approach is able to reduce the phase oscillations considerably within a large domain, as apparent from Fig. 4.5. Unfortunately, as can be seen in Fig. 4.6a this method also yields results that are even worse than those of the piecewise spectrum-guided-integration.

Another contraindication is that this method yields by far the worst results in terms of performance, see the comparison in Fig. 4.6b.

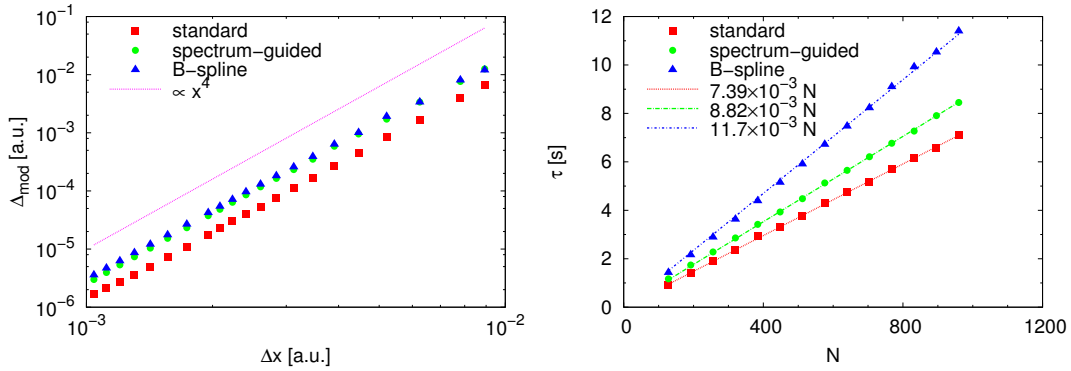

(a) Modulus error **(b)** Time scaling

Figure 4.6: Modulus error Δ_{mod} at the end of the integration for various representations. The softcore potential parameters were $\zeta = \sqrt{2}$, $Z = -1$. The laser wave length was $\lambda = 3000$, its field strength $E_0 = 0.12$. $N = 512$ grid points were used.

Conclusion The optimization strategies based on gauge transformations showed to be ineffective in this example. This is believed to be a consequence of the very sparse escaping density flux. The spectrum-guided-integration and the phase fit method can only work effectively for a high momentum.

4.3 Time dependent scattering event

As a final example, a scattering event is considered. A softcore potential is taken as the central potential again. This time, we have $Z = 18$ and $\zeta = \sqrt{2}$. An initial gaussian wave packet with $x_0 = 10$, $p_0 = -5$ and $\sigma_x = 1$ will be scattered off the potential. The potential and the wave packet are defined as before, see Eqs. (4.20) and 4.4.

The Hamiltonian of this system is time-independent, which means that the energy spectrum is conserved. Hence, the temporal variant $g_{\overline{E}}$ of the spectrum-guided-integration is again rather uninteresting and will not be examined. Instead the spatial piecewise spectrum-guided-integration as well as a B-spline phase fit gauge will be compared to the standard gauge. Again, the phase fit will be performed using quadratic B-splines and $N_{\text{break}} = 4$ break points.

Figure 4.7 shows that the wave packet is split into two major fractions after the scattering. One part goes through the potential while another part is reflected. Due to this clear splitting, the phase fit is expected to be the best choice among the discussed gauge strategies.

In Figs. 4.8 the momentum distributions are illustrated in both the standard and the phase fit representations. In the standard representation the momentum shows two distinct bands after the collision with the potential. The phase fit on the other

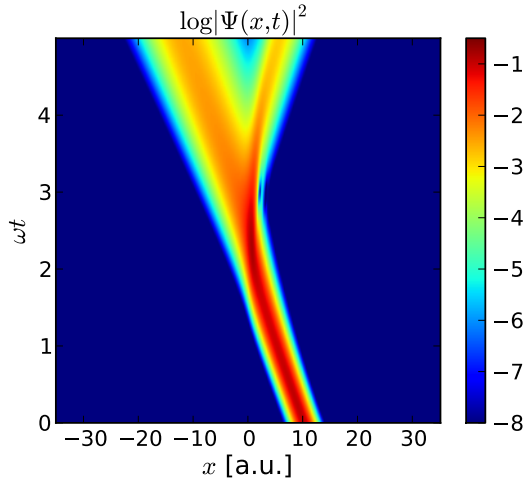

Figure 4.7: Spatial time evolution of an initial gaussian wave packet which scatters off a central softcore potential. A considerable amount of the wave function is reflected, while another part goes through the potential.

hand transforms this distribution in a way such that there is only a single momentum band in the center.

The maximum error Δ_{mod} of the absolute of the wave function, see Eq. (4.13), can be compared in Fig. 4.9a. Only a small advantage can be gained from the spectrum-guided-integration, compared to the standard representation. The B-spline phase fit, however, is able to reduce the error by a factor of $\epsilon/\epsilon' \approx 30$ at the same grid resolution.

Unfortunately, this is also accompanied by a massive increase in computational time, see Fig. 4.9b. For the same N the phase fit almost doubles the costs of the standard time evolution. This nearly annihilates the effective gain in computation time.

The worst option, however, is the spectrum-guided-integration in this respect. Giving only a very slight improvement in accuracy, the computation times are increased by $\tau'/\tau > 1.2$.

Scheme	$\epsilon(N)/\epsilon_0(N)$	$\tau(N)/\tau_0(N)$	$\tau(\epsilon)/\tau_0(\epsilon)$
spectrum-guided	0.44	1.2	1.0
B-spline fit	0.033	1.8	0.76

Table 4.1: Comparison of the computational performance of piecewise spectrum-guided-integration and the B-spline phase fit method. The values are approximate averages. The last column is computed assuming a scaling of $\epsilon \sim \Delta x^4$.

It should be stated that the implementations of the schemes were very straightforward. No special care was taken to optimize the performance. This means that it should be possible to improve the performance of the piecewise spectrum-guided-

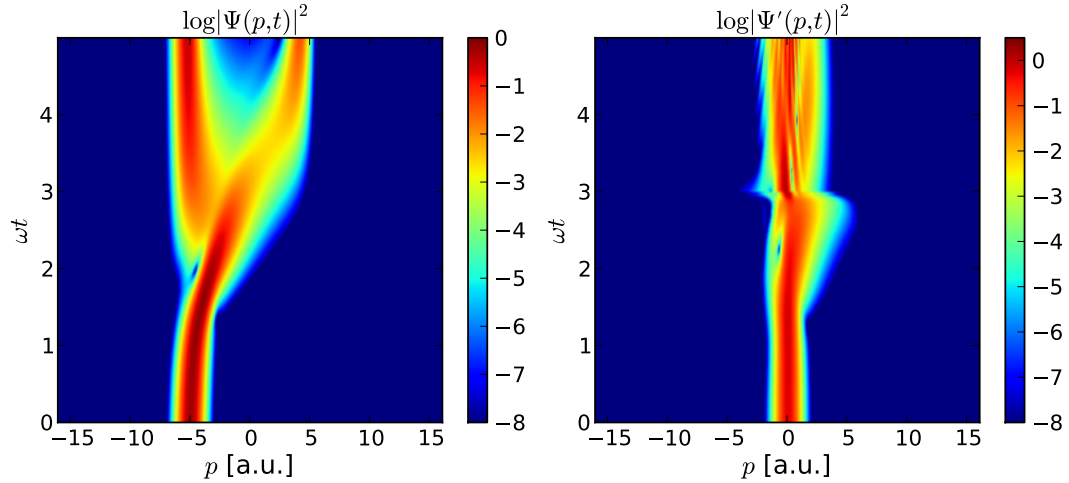

(a) Standard gauge **(b)** B-spline fit gauge

Figure 4.8: Time evolution in momentum space for a gaussian wave packet which scatters off a central softcore-potential. The momentum distribution is evaluated (a) in standard representation and (b) using the B-spline phase fit method.

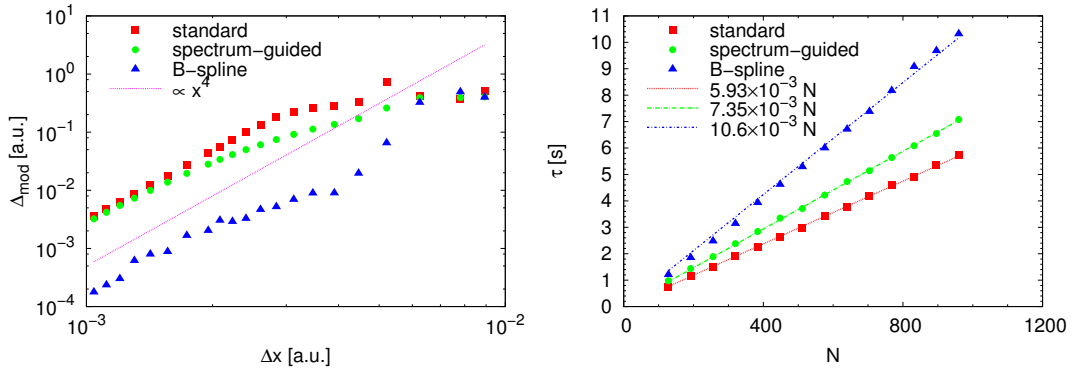

(a) Modulus error **(b)** Computation time

Figure 4.9: Numeric performance of standard gauge, spatial piecewise spectrum-guided-integration and B-spline phase fit method.

integration and especially the phase fit implementations. Also the number of timesteps for each gauge interval $M = 25$ was very small and can probably be increased without loss of accuracy. On this basis the $\tau(\epsilon)$ dependency can probably be improved.

5 Conclusions

The spectrum-guided-integration provides a powerful mechanism to reduce errors in the numerical integration of the Schrödinger equation. However, its applicability and effectiveness is restricted to systems, where a classical solution is available and the system behaves much like the classical analogon. In this thesis, two extensions of the method to overcome these limitations were developed and applied.

First, a piecewise application of the spectrum-guided-integration was discussed. The advantage of this method is that it works without prior knowledge of the center-of-mass motion. The employed gauge functions depend on a constant-in-time energy and momentum parameter. Both of these can be measured as the corresponding expectation value at the beginning of the gauge interval. The effect of such transformations was reasoned to be a mere shift in the energy and momentum spaces respectively.

Second, a generalization to the spectrum-guided-integration was proposed, which can work for broad-band momentum distributions. The idea is to interpolate or approximate the phase $\arg \Psi(\boldsymbol{x}, t)$. This also shifts the momentum expectation value towards zero. In addition, the momentum distribution is deformed, depending on the fit function.

An error estimation was performed. It was demonstrated that the accuracy can be improved due to the gauge-transformed modelling. The accuracy gain due to the gauge-transformed modelling is an increasing function of the mean momentum in the original system divided by its width.

Finally, to illustrate and test the considerations, the methods were applied on three model systems. The effects of the transformations were illustrated in the framework of these systems. Benchmarks and accuracy were evaluated and compared.

In a harmonic oscillator the piecewise spectrum-guided-integration could be shown to be efficient. Spatial oscillations in the transformed system were reduced considerably. The computational time for the same resulting accuracy could be improved by a factor of approximately five.

The second system was a bound state in a softcore potential, which was exposed to a laser for a limited timespan. In this system, all of the proposed methods were tried out. The piecewise spectrum-guided-integration proved to be ineffective. Probably, this is due to the fact that the mean momentum of the system was approximately zero to start with. An interpolation of the phase function turned out to be highly unstable after just a few number of time steps. The reason for the instability could not be determined in detail. The suspicion is that it originates from the highly $\boldsymbol{x}$-dependent behaviour in the peripheral areas. Finally the phase function was approximated using a B-spline fit. This method was expected to overcome the problems of both previous attempts. In fact the spatial oscillations could be reduced considerably. In spite of

this the accuracy was not improved. In terms of performance this method was very inefficient.

For the third system a softcore potential was taken again as the central potential. This time an initial gaussian wave packet scattered off this central potential. In the context of this system, the phase fit method turned out to yield very good results. In comparison to the spectrum-guided-integration and the ordinary gauge, the error accuracy could be improved by a factor of about 30. This value is obtained by comparing the errors emerging at the same grid resolution. However, the implementation of the phase fit method scales very bad with respect to computation time. The effective reduction of the computation time for the same error is given by $\tau'_\epsilon/\tau_\epsilon \approx 0.76$.

The usage of more sophisticated heuristics for the piecewise spectrum-guided-integration remains subject to further investigations. Such may include a nonlinear prognosis of the center-of-mass motion. This can allow to prolong the gauge interval during which the transformation yields good numerical results. It is also desirable to predict how long a particular gauge remains effective.

Another subject to further investigation is the choice of the fit function for the phase fit gauge. A targeted choice may be used to deform the momentum spectrum in a controlled way. For the B-spline fit itself the order of the basis functions, the number of breakpoints as well as the knots distribution pose additional degrees of freedom, which were not investigated here.

Bibliography

[1] G. E. Kimball and G. H. Shortley. The Numerical Solution of Schrödinger's Equation. *Phys. Rev.*, 45:815–820, Jun 1934.

[2] C. Leforestier, R. H. Bisseling, C. Cerjan, M. D. Feit, R. Friesner, A. Guldberg, A. Hammerich, G. Jolicard, W. Karrlein, H. D. Meyer, N. Lipkin, O. Roncero, and R. Kosloff. A Comparison of Different Propagation Schemes for the Time Dependent Schrödinger Equation. *Journal of Computational Physics*, 94(1):59–80, May 1991.

[3] H. G. Muller. An Efficient Propagation Scheme for the Time-Dependent Schrödinger Equation in the Velocity Gauge. *Laser Physics*, 9(1):138–148, Jan-Feb 1999.

[4] Heiko Bauke and Christoph H. Keitel. Canonical transforms and the efficient integration of quantum mechanical wave equations. *Physical Review E*, 80(1), Jul 2009.

[5] P. Ehrenfest. Bemerkung über die angenäherte Gültigkeit der klassischen Mechanik innerhalb der Quantenmechanik. *Zeitschrift für Physik A Hadrons and Nuclei*, 45:455–457, 1927. 10.1007/BF01329203.

[6] Franz Schwabl. *Quantum Mechanics*. Springer, 4th edition, November 2007.

[7] Philip Pechukas and John C. Light. On the Exponential Form of Time-Displacement Operators in Quantum Mechanics. *The Journal of Chemical Physics*, 44(10):3897–3912, 1966.

[8] Abdul J. Jerri. The Shannon Sampling Theorem – Its Various Extensions and Applications - A Tutorial Review. *Proceedings of the IEEE*, 65(11):1565–1596, 1977.

[9] Claude E. Shannon. Communication in the Presence of Noise. *Proceedings of the IRE*, 37(1):10–21, 1949.

[10] J. L. Brown, Jr. On the error in reconstructing a non-bandlimited function by means of the bandpass sampling theorem. *Journal of Mathematical Analysis and Applications*, 18(1):75–84, 1967.

[11] Toshiaki Iitaka. Solving the time-dependent Schrödinger equation numerically. *Physical Review E*, 49(5, Part b):4684–4690, May 1994.

[12] William H. Press. *Numerical recipes: The art of scientific computing*. Cambridge University Press, 3rd edition, Sep 2007.

[13] Abraham Goldberg, Harry M. Schey, and Judah L. Schwartz. Computer-Generated Motion Pictures of One-Dimensional Quantum-Mechanical Transmission and Reflection Phenomena. *American Journal of Physics*, 35(3):177–186, 1967.

[14] W. van Dijk and F. M. Toyama. Accurate numerical solutions of the time-dependent Schrödinger equation. *Physical Review E*, 75(3, Part 2), Mar 2007.

[15] Carl de Boor. *A practical guide to splines*. Springer Verlag, 1978.

[16] GSL Project Contributors. GSL - GNU Scientific Library - GNU Project - Free Software Foundation (FSF). http://www.gnu.org/software/gsl/, 2010.

[17] E. H. Kennard. Zur Quantenmechanik einfacher Bewegungstypen. *Zeitschrift für Physik A Hadrons and Nuclei*, 44:326–352, 1927. 10.1007/BF01391200.

[18] Kaimin Fan, Yujun Zheng, Weiyi Ren, and Shiliang Ding. Exact quantum solutions of general driven time-dependent quantum quadratic system. *International Journal of Quantum Chemistry*, 107(7):1355–1366, 2007.

[19] Qiong-Gui Lin. Wave packets of a harmonic oscillator with various degrees of rigidity. *Chinese Journal of Physics*, pages 387–94, 2002.

[20] Abraham Goldberg and Judah L. Schwartz. Integration of the Schrödinger equation in imaginary time. *Journal of Computational Physics*, 1(3):433–447, 1967.

[21] K.E. Schmidt, P. Niyaz, A. Vaught, and M.A. Lee. Green's function Monte Carlo method with exact imaginary-time propagation. *Physical Review E*, pages 16707–1–17, Jan 2005.

Selbstständigkeitserklärung
Ich versichere, dass ich diese Arbeit selbstständig verfasst und keine anderen als die angegebenen Quellen und Hilfsmittel benutzt habe.

Declaration of independence (Guttenberg-clause)
In the name of our fathers and forefathers, I swear the holy oath that I have done this work by myself and only by myself. I have used no other than the listed material and resources so help me god.

Heidelberg, ...